Strength evolution of ice plume deposit analogs of Enceladus and Europa

M. Choukroun[1], J.L. Molaro[1,2], R. Hodyss[1], E. Marteau[1], P. Backes[1], E.M. Carey[1], W. Dhaouadi[1,3], S. Moreland[1], E.M. Schulson[4]

[1]Jet Propulsion Laboratory, California Institute of Technology, Pasadena, CA.

[2] Planetary Science Institute, Tucson, AZ.

[3] ETH Zürich, Zurich, Switzerland.

[4] Thayer School of Engineering, Dartmouth College, Hanover, NH.

Corresponding author: Mathieu Choukroun (Mathieu.Choukroun@jpl.nasa.gov)

Key Points:

- The cone penetration resistance of fine-grained porous ice held under isothermal conditions increases linearly over time.

- The temperature dependence of the strengthening rate yields an activation energy similar to self-diffusion at the surface of ice grains.

- Plume deposits would remain weak on Enceladus, while they may develop substantial strength within a few million years on Europa.

1   **Abstract (150 words limit)**

2   Enceladus and possibly Europa spew materials from their internal ocean into their exosphere,

3   some of which are deposited back onto the surface of those Ocean Worlds. This setting provides

4   a unique opportunity to seek traces of past or extant life in ice plume deposits on their surfaces.

5   However, the design of lander missions and surface sampling techniques, and the choice of

6   sampling locations rely heavily on strength expectations. Here we present an experimental

7   investigation of the evolution in strength of ice plume deposit analogs at several temperatures, as

8   well as a model that predicts first-order estimates of the strength of evolved ice plume deposits

9   under geologic timescales relevant to Enceladus and Europa. These results suggest that plume

10   deposits remain weak and poorly consolidated on Enceladus, while they may develop substantial

11   strength (comparable to solid ice) within < 100 My on Europa.

12

13   **Plain Language Summary**

14   Enceladus and Europa are Ocean Worlds; they harbor an internal ocean beneath their ice shells.

15   There is proof that plumes emit ocean materials out of Enceladus, similar to geysers on Earth,

16   and some evidence for a similar activity at Europa. Based on the composition of the plumes and

17   the surface, both Enceladus and Europa are the leading outer Solar System candidates for

18   possibly harboring life. Areas where fresh plume materials are deposited would be the best

19   location to search for traces of life on the surface. A major challenge in preparing mission

20   concepts to explore these locations arises from the need to collect samples of the surface ice,

21   while little is known at present about the mechanical properties of the surface. In this study, we

22   prepared icy plume deposit analogs, and let them evolve in the laboratory over extended periods

23   of time to investigate the evolution of their strength over time. We find that plume deposits are

24   likely to remain loose and exhibit a low strength over geologic timescales under Enceladus

25   conditions, suggesting they would be relatively easy to sample. Conversely, under Europa's

26   surface conditions, such plume deposits appear likely to develop a substantial strength.

27 **1. Introduction**

28 Enceladus and Europa are viewed as the most likely Ocean Worlds to be habitable, and perhaps

29 inhabited. Their internal ocean is likely in direct contact with the silicate interior (Anderson et

30 al., 1998; Sotin & Tobie, 2004; Schubert et al., 2007; Iess et al., 2014), possibly favoring the

31 development of hydrothermal systems (Zolotov & Shock, 2001b; Glein et al., 2008; Zolotov &

32 Kargel, 2009; Sohl et al., 2010; Sekine et al., 2015) similar to those found on Earth, which may

33 be the source of nutrients and energy for prebiotic chemical reactions that could lead to the

34 emergence of life.

35 Enceladus is the only Ocean World where current geologic activity undoubtedly emits

36 materials from the internal ocean into its exosphere. *Cassini* observed multiple jets converging

37 into a plume (Porco et al., 2006), which originates from a set of four rectilinear surface fractures

38 dubbed Tiger Stripes (Spitale & Porco, 2007). Enceladus' plume consists of micron-size particles

39 mostly comprised of water ice that feed Saturn's E ring (Kempf et al., 2010). These particles also

40 contain percent-level NaCl (Postberg et al., 2009; Postberg et al., 2011) and complex organic

41 materials (Postberg et al., 2018). The plume contains volatiles such as ammonia, carbon dioxide,

42 low-mass organics, ^{40}Ar (Waite et al., 2009), and molecular H_2 (Waite et al., 2017). The

43 moderately high pH derived for the ocean (Glein et al., 2015), the plume composition, and the

44 abundant geologic energy from the interior and within the South polar terrain entice the prospect

45 that life may have emerged and still be present on Enceladus (McKay et al., 2008; McKay et al.,

46 2014; McKay et al., 2018).

47 Europa's surface bears evidence for activity in the recent geologic past and a strong

48 habitability potential. Its surface age is estimated to 60-100 My (Zahnle et al., 2008; Bierhaus et

49 al., 2009). Geochemical modeling of water-rock interactions suggests that Europa's internal

50 ocean may be habitable (Zolotov & Shock, 2001b; Zolotov & Shock, 2001a, 2003; Zolotov &

51 Kargel, 2009). The characterization of possible present-day plume activity at Europa is still an

52 area of active research (Roth et al., 2014; Sparks et al., 2016; Jia et al., 2018; Paganini et al.,

53 2019). The *Europa Clipper* mission (Pappalardo et al., 2015), in development at time of writing,

54 is equipped to detect and analyze such plumes. Until more definitive information is available, it

55 seems reasonable to consider that Europa may emit materials from its internal ocean in a manner

56 akin to Enceladus.

57   *Cassini* observations of Enceladus plume particles enabled the determination of their
58   grain size distribution, their trajectories, and their deposition back onto the surface. The mean
59   radius of equivalent-sphere particles determined from imaging is 3.1 ± 0.5 μm (Ingersoll &
60   Ewald, 2011). A particle ejection model was derived from the vertical structure of the plume
61   (Schmidt et al., 2008). The deposition of plume particles can then be computed as function of
62   particle size, source location, and location on the Enceladus surface (Kempf et al., 2010;
63   Southworth et al., 2019). Particles with radii $0.1 - 5$ μm are expected to dominate the plume
64   deposits. The deposition rate averages on order of 1 μm/yr across the entire Enceladus surface,
65   but can be up to 1 mm/yr in locations close to jet sources.

66   Plumes on Enceladus and perhaps Europa could carry biosignatures, or even microbial
67   life forms, and deposit them on their surface (Porco et al., 2017). Other extrusion mechanisms
68   have also been proposed on Europa, such as diapirism (Pappalardo & Barr, 2004). The prospect
69   of finding life, or traces of it, on Europa and Enceladus has motivated the development of
70   mission concepts to explore their surface (Hand, 2017). At time of writing, an Enceladus mission
71   concept is under study to support the upcoming Planetary Science and Astrobiology Decadal
72   Survey for 2023-2032.

73   Plume deposits would consist of ice particles that form a granular unconsolidated
74   material, which may subsequently evolve over time in a fashion similar to snow on Earth. Snow
75   undergoes a sintering process, in which redistribution of water molecules between grains initiates
76   bonding between grains at their neck, and continues to evolve into a dense material such as in
77   glaciers (Blackford, 2007). However, melting and refreezing processes play an important role in
78   the evolution of snow, making it a relatively poor analog. Sintering of ice particles in planetary
79   environments is the subject of active research (Molaro et al., 2019). Mass redistribution of ice
80   and growth of the contact regions between grains is anticipated, while a high bulk porosity could
81   be retained over long timescales. The mechanical properties of fine-grained plume deposits
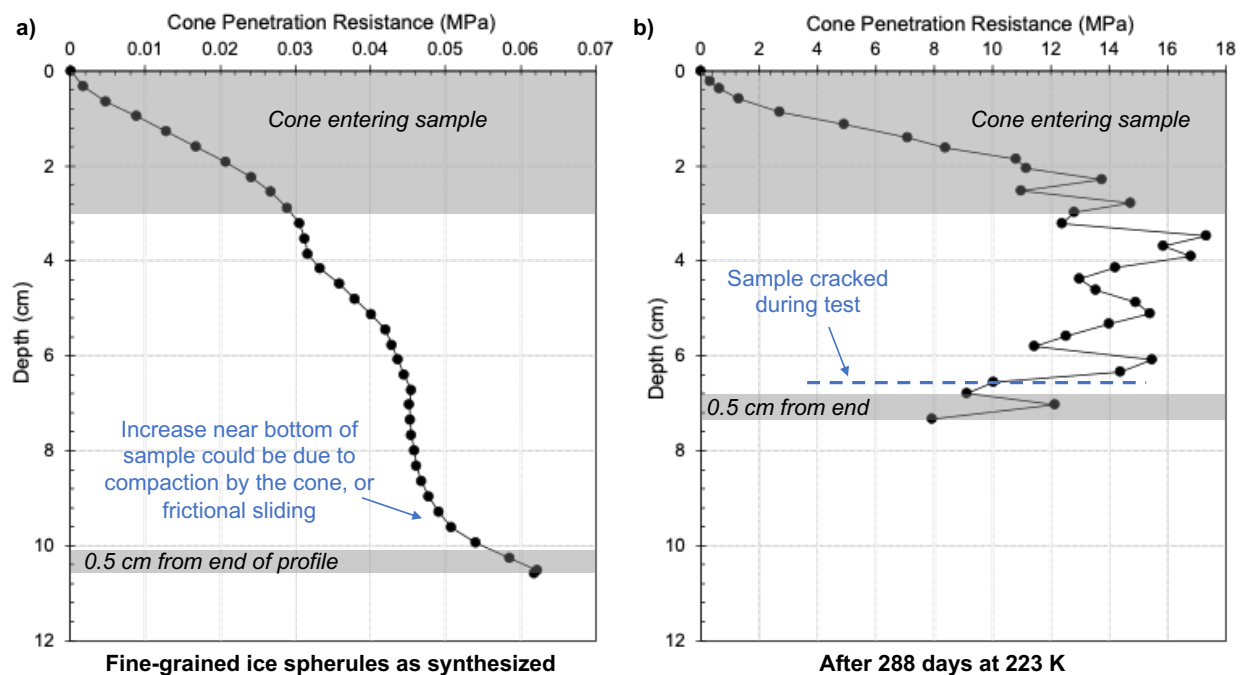82   under Enceladus and Europa's surface conditions are poorly constrained to date.

83   This article presents the first laboratory study of the time evolution of the mechanical
84   properties of fine-grained ice particles similar to those of Enceladus' plume at a range of
85   temperatures. We derive the rate of strengthening and its temperature dependence from these
86   measurements, then extrapolate the results to Europa and Enceladus' surface conditions to
87   estimate and compare the mechanical properties of plume deposit regions on these two bodies.

88

2. Mechanical resistance of ice plume deposit analogs

89

90 Fine-grained (12 μm mean diameter particles) crystalline ice was synthesized by air atomization

91 and deposition in liquid nitrogen. Large samples of unpacked ice particle aggregates (porosity of

92 51.5 +/- 1.6 %), weighing between 0.66 and 2.14 kg each, were left to sinter in sealed containers

93 under isothermal conditions (193 K, 223 K, 233K, 243 K) for periods of time ranging from a few

94 months up to 14 months, depending on temperature. The mechanical strength of the samples was

95 measured routinely using a custom-built cone penetrometer apparatus. A complete description of

96 materials and methods, and a summary of experiments and samples are presented in

97 Supplementary Information (Text S1, Figures S1-S3, Tables S1-S2).

98

99

Figure 1. Examples of cone penetration resistance profiles from two end-member situations: *a)* ice just after sample preparation, *b)* ice sintered for 288 days at 223 K. In all profiles, the first 3 cm and the last 0.5 cm in the profiles (which may be within 3 cm from bottom of the container) are not representative of the samples' strength. Note the increase in resistance of more than 2 orders of magnitude upon sintering over 9.5 months at 223 K.

104

105 Every time a cone penetration test was conducted on a sample, we obtained a cone

106 penetration resistance profile as function of depth within the probed portion of sample. Two

107 example profiles are illustrated in Figure 1 and show extreme end-members of strength profiles

108   obtained. The weakest measurement is from an ice sample just after synthesis (Figure 1-a), and

109   the strongest is from an ice sample that spent 288 days at 223 K (Figure 1-b).

110   The average resistance of each cone penetration profile was derived as follows. The

111   initial contact of the cone penetrometer with the samples (upper ~ 3 cm) was neglected, since the

112   plastic zone that forms around the cone tip as it passes through the material has not fully

113   developed yet (Rogers, 2006). The bottom 0.5 cm of the strength profiles was also excluded, as

114   we stopped the cone penetrometer ~ 3 cm from the bottom of the sample containers during

115   measurements. The mean value of the strength profile in the remaining mid-section of the

116   samples, between 3 cm and approx. 9 cm depth (3 cm from container bottom), was then taken to

117   be representative of the average strength of the sample in that profile. The error on each average

118   strength measurement was derived from the 1-σ standard deviation around this mean value.

119

120   **3. Strength evolution of plume deposit analogs upon sintering**

121   Figure 2-a shows the evolution in average cone penetration resistance of all ice samples. One

122   sample at 223 K exhibited a different strength evolution from the others and was discarded in the

123   analysis (Text S2). At each temperature, strengthening is observed over time and forms

124   seemingly linear trends, which we constrained through a linear regression that included

125   weighting by error bars on individual data points. Table S3 reports the numerical values of fit

126   parameters at each temperature and their 2σ errors. The best-fit parameters yield trend lines that

127   do not encompass the strength of the fresh ice samples, which suggests some early strengthening,

128   perhaps associated to a different process in the evolution of the samples. We have not attempted

129   to further refine fits, because this effect is only obvious at the warmer temperatures, and the

130   dispersion within the dataset is such that more complex fit functions would not have a greater

131   probability of accurately fitting the data.

132   An Arrhenius plot shows in Figure 2-b the natural logarithm of the rate of strengthening

133   as function of inverse sample temperature. The error bars correspond to the 95% confidence

134   interval of the strengthening rate at each temperature. The four data points follow a line in this

135   representation, whose slope is by definition -Q/R, where Q is the activation energy of the

136   considered rate as function of temperature, and R is the ideal gas constant 8.314 J/(mol.K). A

137   linear regression of the dataset, weighted by the standard deviation of the measurements, yields

138   an activation energy Q = 24.3 ± 3.3 kJ/mol (95% confidence interval).
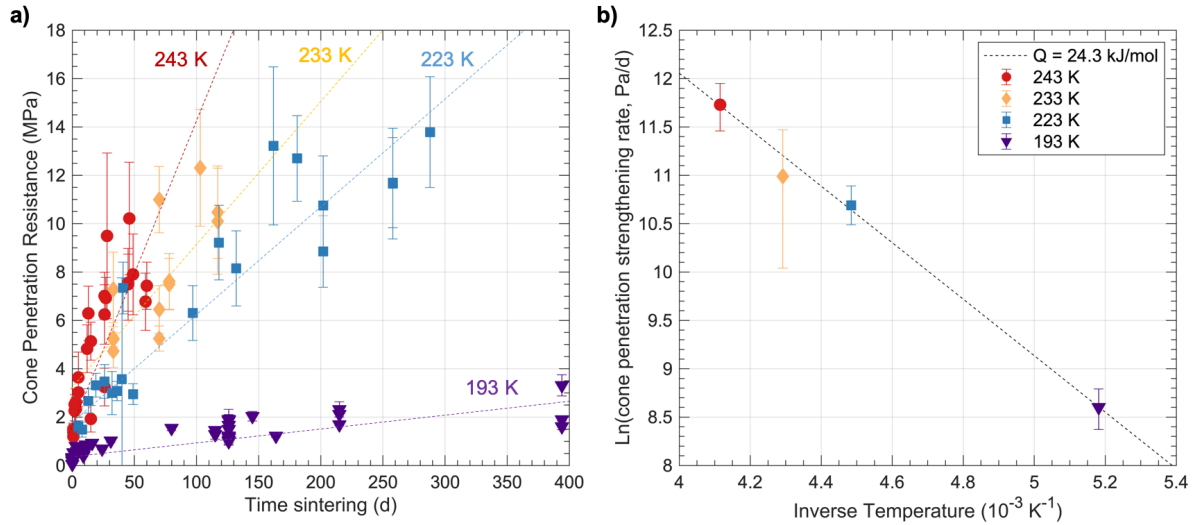
139

141   **Figure 2.** Measured evolution in cone penetration resistance of all samples as function of time *(a)*, and Arrhenius plot
142   of rate of strength increase as function of inverse temperature *(b)*. Slopes of linear trends derived from
143   measurements at each temperature *(a)* are used to derive the activation energy *(b)* that represents the effect of
144   temperature on these rates, and enables extrapolation to colder temperatures (Section 5).

145

146   This activation energy is comparable to that of the strength of hydrogen bonds (Suresh &

147   Naik, 2000), as well as to the activation energy of H_2O self-diffusion on the surface of ice grains

148   (Nasello et al., 2007). It is not consistent with the activation energy associated with ice

149   recrystallization, or with the volume or vapor diffusion mechanisms that contribute to the

150   sintering process (Molaro et al., 2019). This suggests that the strengthening of fine-grained ice

151   deposits upon sintering is primarily due to the evolution of a mesoscale network between

152   individual grains, or agglomerates thereof.

153

154   **4. Implications for mechanical behavior of ice plume deposit analogs**

155   The two cone penetration resistance profiles shown in Figure 1 seem to indicate different kinds

156   of mechanical response during testing between unconsolidated and heavily sintered ice. One kind

157   is exhibited by aggregates of either little or no cohesion amongst grains and is characterized by a

158   very low average cone penetration resistance, that nevertheless increases roughly linearly with

159   depth (Figure 1-a). This is reminiscent of the behavior of dry, polar snow of similar density

160   (McCallum, 2012; McCallum, 2014). The other kind is exhibited by aggregates comprised of

161   grains that, through the temporally and thermally dependent process of sintering, develop

162   significant cohesion amongst themselves and thus possess a much higher collective resistance,

163   around 14 MPa in the example shown in Figure 1-b. This resistance, while oscillating, is more or

164   less independent of depth once the cone has penetrated some distance into the material. The two

165   kinds of mechanical behavior likely originate from different grain-scale interactions.

166   We examined the strength-depth correlation factor and the relative dispersion within each

167   of the 100 cone penetration profiles obtained, in order to investigate whether the difference in

168   behavior is well represented in our dataset and to constrain the stage of consolidation (cone

169   penetration resistance) at which a transition between deformation regimes may occur. The

170   relative dispersion is the ratio of the standard deviation in cone penetration resistance over the

171   mean cone penetration resistance in each profile. The strength-depth correlation factor κ relates

172   strength S and depth x in each profile, and may indicate depth-strengthening (positive values) or

173   depth-weakening (negative values) behaviors. κ is expressed as follows:

174     $$\kappa = \frac{\sum_i (S_i - \bar{S})(x_i - \bar{x})}{\sigma_S \sigma_x} \qquad (2)$$

175   where S_i and x_i indicate the individual measurements of strength and depth along the

176   profile, respectively, $\bar{S}$ and $\bar{x}$ are the mean strength and mean depth of the profile, respectively,

177   and σ_S and σ_x are the standard deviation around the mean strength and mean depth, respectively.

178   At first sight, the strength-depth correlation factor (Figure 3-a) and the relative dispersion

179   (Figure 3-b) may seem mostly scattered throughout the dataset. However, very high positive

180   correlation factor values (depth-strengthening) are clustered at resistances below 2 MPa. Also, an

181   increasing trend in relative dispersion with resistance is observed. Although the increase in

182   relative dispersion throughout the range of measured cone penetration resistances is smaller than

183   the total dispersion of the dataset ($\sigma = 0.1$), the mean relative dispersions at resistances < 1 MPa

184   and > 2 MPa are separated by more than one standard deviation of these two populations ($\sigma \sim$

185   0.05 in both). These observations suggest that a transition between mechanical behaviors could

186   be reflected in the dataset at the low end of measured cone penetration resistance values.

187   The distribution of strength-depth correlation factor and relative dispersion within three

188   ranges of cone penetration resistance (below 1MPa, 1-2 MPa, above 2 MPa) point to a transition

189   in mechanical behavior around 1-2 MPa in our samples (Figure 3-c and 3-d). For resistance < 1

190   MPa, the correlation factor indicates a depth-strengthening behavior, and the relative dispersion

191   is dominated by a mode centered around 0.05-0.1, although a second mode is visible. For

192   resistance in the range 1-2 MPa, the depth-strengthening behavior does not dominate anymore,

193   while the relative dispersion shows a decrease in frequency of low-end values and an increase in

194   frequency of the second mode, centered around 0.15-0.2. For resistance > 2 MPa, the correlation

195   factor appears uniformly distributed, while the relative dispersion only exhibits the second mode

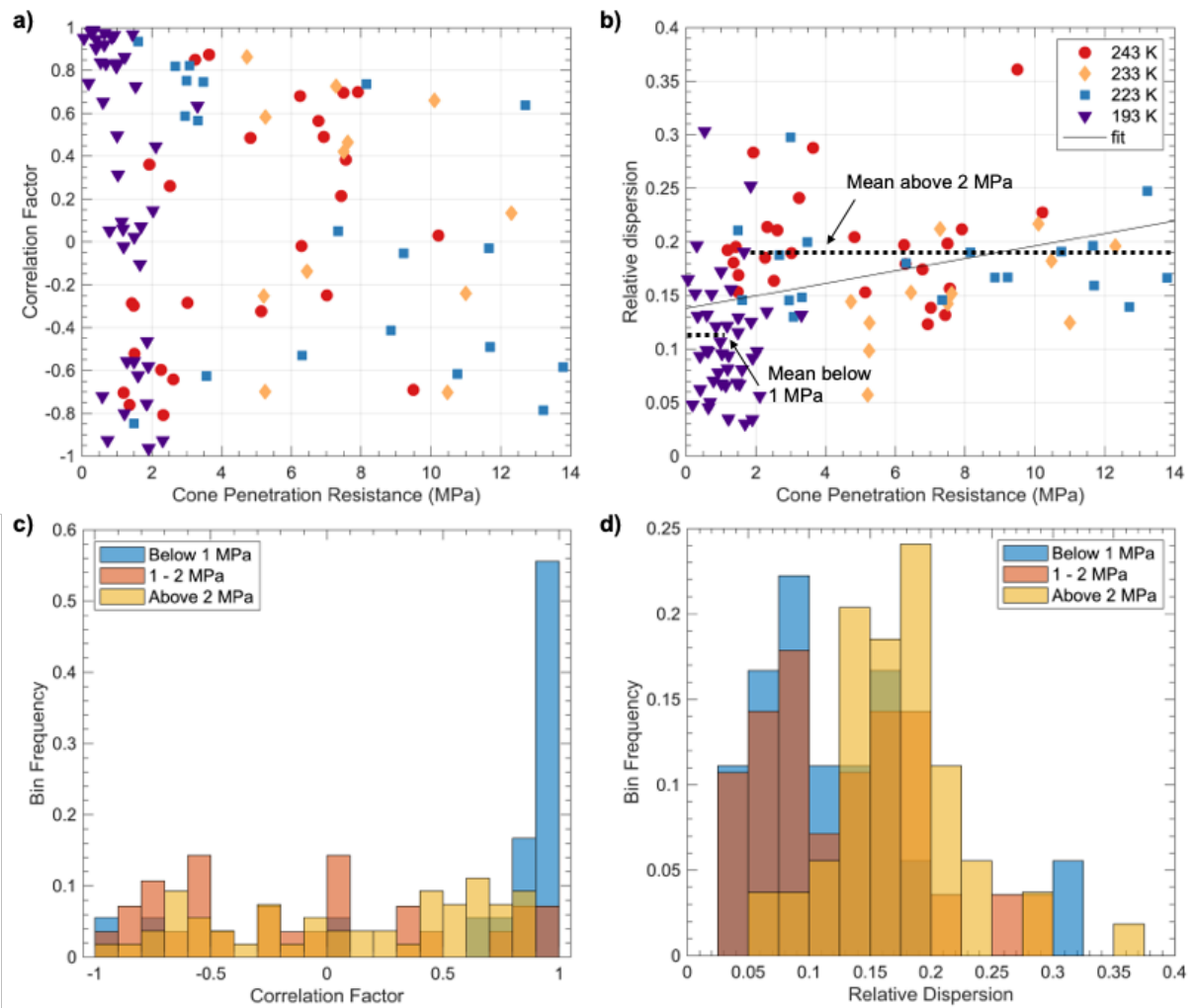196   that is consistent with the mean value of 0.19 above 2 MPa.

197

198

199   **Figure 3.** *(a)* Strength-depth correlation factor as function of cone penetration resistance for all profiles. Color coding
200   follows temperature as in panel *(b)*. *(b)* Relative dispersion (standard deviation over cone penetration resistance) as
201   function of cone penetration resistance for all profiles; one outlier is not shown. These datasets, along with
202   histograms of the distribution of correlation factor *(c)* and relative dispersion *(d)* within different ranges of cone
203   penetration resistance, suggest a transition between two different mechanical behaviors around 1-2 MPa.

204

205   The two kinds of mechanical behaviors can be interpreted as follows: response of an

206   unconsolidated aggregate of ice grains below 1 MPa, and brittle compressive failure of a

207   consolidated aggregate above 2 MPa. Below 1 MPa, the linear increase in resistance with depth

208   (Figure 1-a) is consistent with high positive values of the strength-depth correlation factor. This

209   linear increase has been observed in other cone penetration and micropenetrometer

210   measurements conducted in dry, polar snow, where it was attributed to frictional sliding of

211   unconsolidated ice against the steel rod as the cone-rod assembly advanced (McCallum, 2012;

212   McCallum, 2014), and to compaction of the unconsolidated ice ahead of the cone (van

213   Herwijnen, 2013). Above 2 MPa, brittle compressive failure of the cohesive aggregate, in which

214   a rigid network has already developed between grains to the scale of the samples, would explain

215   all findings in that regime: the jerky indentation seen in cone penetration profiles (Figure 1-b),

216   the approximately constant relative dispersion, the absence of strength-depth correlation, and a

217   resistance of overall magnitude comparable to the brittle compressive strength of ice. Future

218   studies investigating the transition between mechanical behaviors may refine this interpretation.

219

220   **5.   Implications for strength of surface plume deposits on Enceladus and Europa**

221   The cone penetration resistance of icy plume deposit analogs increases linearly over time at a

222   given temperature (Section 3). Using the activation energy Q derived from our dataset, the rate

223   of strengthening $r_S(T)$ at a given temperature can be predicted by:

224    $$\ln r_S = \ln r_0 - \frac{Q}{RT} \qquad\qquad (2)$$

225   where r_0 is the intercept of the rate of strengthening determined from the Arrhenius plot

226   (Figure 2-b).

227   This Arrhenius expression necessarily assumes that the evolution of the strengthening

228   rate can be reliably extrapolated outside of the temperature range where it was derived from the

229   experimental data (Figure 2). This assumption appears justified to derive at least an upper bound

230   of the resistance of these materials for the following reasons. 1) The surface of Enceladus is

231   dominated by the same hexagonal ice I_h as used in our experiments (Filacchione et al., 2007;

232   Filacchione et al., 2010). 2) The surface of Europa may contain a small fraction of amorphous

233   ice due to irradiation effects, but it appears nevertheless dominated by ice I_h (Hansen & McCord,

234   2000; Berdis et al., 2020). 3) Low H_2O vapor pressure and airless conditions at the surface of

235 Europa and Enceladus would ease release and escape of H_2O, which suggests that ice could

236 redistribute less efficiently within plume deposits than in our experiments.

237   Figure 4 explores how the strengthening rate from the experimental data evolves under

238 the surface conditions of Europa and Enceladus. Approximate temperature ranges at Enceladus

239 are based on *Cassini* data, where South polar terrain mean temperatures can be colder than 50 K,

240 while noontime equatorial temperatures can reach over 80 K (Howett et al., 2010), and

241 temperature at the Tiger Stripes was evaluated to ~ 180 K (Spencer & Nimmo, 2013).

242 Approximate temperature ranges for Europa are based on Galileo data (Spencer et al., 1999). The

243 predicted rates of strengthening as function of temperature for best-fit and ±2σ Q values from

244 Eq. 2 are shown in Figure 4-a. From this, the cone penetration resistance of icy plume deposits is

245 predicted as function of temperature and time (Figure 4-b).
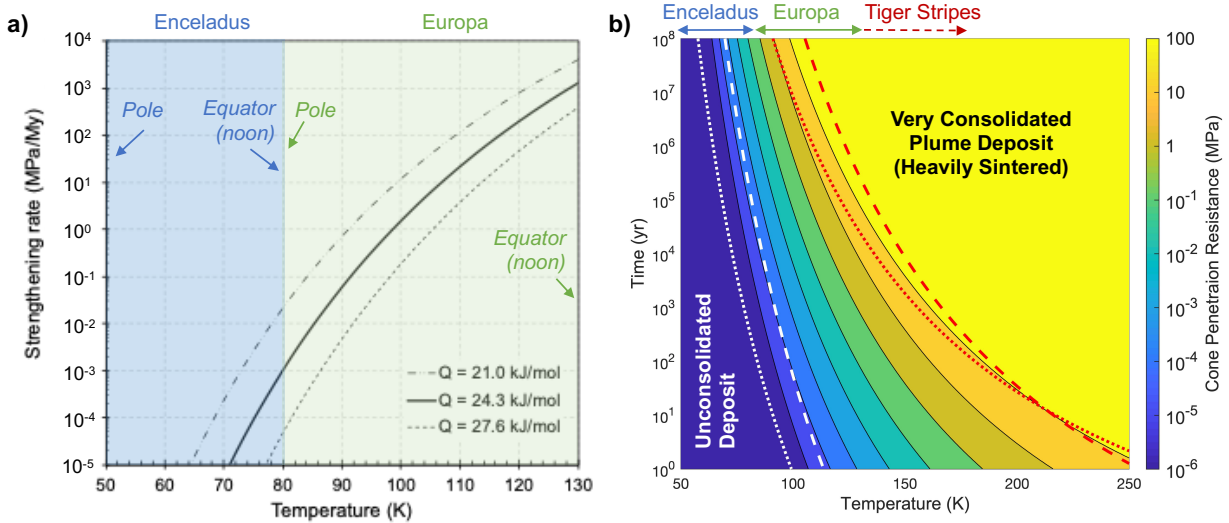
246

Figure 4. *(a)* Predicted strengthening rate of icy plume deposits as function of temperature, for the best-fit activation energy, and for values +2σ and -2σ from it. Representative temperature ranges at equilibrium for polar and equatorial midday conditions on Enceladus and Europa are illustrated for comparison. *(b)* Predicted cone penetration resistance of icy plume deposits as function of temperature and sintering time. Black contours are for the best-fit activation energy value. Dashed and dotted contours illustrate the effect of the uncertainty on activation energy of +2σ and -2σ, respectively. For legibility, these contours are only shown for the 10^{-5} (white) and 100 MPa (red) cone penetration resistance levels.

256   It is important to note that our laboratory experiments do not inform whether the

257 strengthening rate eventually decreases and an ultimate cone penetration resistance value may be

258 reached, which would be expected once ice sintering nears completion. The highest resistance

259 recorded in our experiments was 14 MPa, but it was still increasing linearly at the time and no

260 densification had yet occurred. For comparison, the uniaxial unconfined compressive strength of

261 compact water ice at 233 K is around 30 MPa (Petrovic, 2003), and it increases with decreasing

262 temperature up to 60-80 MPa at temperatures 70-130 K (Arakawa & Maeno, 1997; Schulson &

263 Duval, 2009). However, the relationship between cone penetration resistance and unconfined

264 compressive strength is not trivial and depends strongly on materials microstructure, test

265 characteristics, and modes of failure. Further investigating this would require a dedicated study

266 and goes beyond the scope of this article. For order of magnitude, we estimate that a cone

267 penetration resistance greater than 10 MPa corresponds to a heavily sintered (albeit still porous)

268 material, and predicted values higher than 100 MPa are not shown in Figure 4-b.

269 Under typical Enceladus surface conditions, little to no strengthening is expected for

270 plume deposits. In the South polar region, it would take at least the age of the Solar system for

271 the deposits to develop a resistance on order of 1 MPa (Figure 4-a). Under Enceladus equatorial

272 noontime temperatures, plume deposits would still take about 100 My for to reach 1 MPa cone

273 penetration resistance. For comparison, our laboratory samples of 1 MPa cone penetration

274 resistance are poorly consolidated, and friable by hand. Thus, plume deposits in these areas are

275 anticipated to remain poorly consolidated and relatively easy to sample.

276 Close to the Tiger Stripes, where temperatures up to 180 K have been estimated (Spencer

277 & Nimmo, 2013), plume deposit materials would develop a cone penetration resistance around

278 10 MPa in ~ 15 years. For comparison, our laboratory samples with a cone penetration resistance

279 on order of 10 MPa are very consolidated. Cracks and faulting planes develop and propagate

280 across the entire samples on failure. Excavating and acquiring samples of such materials would

281 require tools able to break the materials and generate tailings, such as rasps or drills.

282 However, these regions close to the Tiger Stripes are also areas where the deposition of

283 new plume deposits would be most intense, on order of 0.01 to 1 mm/yr (Kempf et al., 2010;

284 Southworth et al., 2019). There would be competition between strengthening of existing plume

285 deposits and covering by new fresh and loose particles, therefore the spatial distribution in

286 deposition rate across the surface could be an important factor for selecting sampling sites.

287 Depending on the local deposition rate and thermal environment, one may seek plume deposit

288 areas that are fresh enough to remain poorly consolidated over the first few centimeters.

289   Europa is an intermediate situation between Enceladus' nominal surface conditions and

290   its hot spots at the Tiger Stripes. Europa's surface temperature ranges from around 80 K in the

291   nighttime up to > 130 K for noon time equatorial temperatures (Spencer et al., 1999), and its

292   annual mean is around 100 K. The expected cone penetration resistance of plume deposits can

293   vary from that of unconsolidated or poorly consolidated ice grains in fresh deposits and/or in the

294   winter polar regions, to that of very consolidated materials in geologically old deposits and/or the

295   equatorial regions. The latter would require a sampling approach that includes means to break up

296   surface materials, collect the tailings and then transfer them for analysis. Such an approach is

297   being considered for the potential Europa lander mission concept, currently in formulation

298   (Hand, 2017).

299

6. Conclusions

301   This study presents the first experimental investigation of the impact of sintering on the strength

302   of bulk ice plume deposit analog samples relevant to Enceladus and Europa. Ice plume deposit

303   analogs were left to sinter under isothermal conditions and at water vapor saturation pressure for

304   up to 14 months. Cone penetration resistance measurements conducted over the course of the

305   experiments showed a linear increase in strength with respect to time at all temperatures. A

306   transition between two mechanical behavior regimes occurs around 1-2 MPa cone penetration

307   resistance. The temperature dependence of the rate of strengthening follows an Arrhenius

308   relationship and yields an activation energy of 24.3 ± 3.3 kJ/mol. This value is consistent with a

309   process dominated by self-diffusion of H_2O molecules on the surface of ice grains. Extrapolation

310   to the surface conditions of Enceladus and Europa suggests that little strengthening would occur

311   on Enceladus, except in hot spot regions that do not experience subsequent deposition of fresh

312   plume particles, while substantial strengthening may occur on Europa over geologic timescales.

313   At a time where the surface and subsurface exploration of Ocean Worlds is a high

314   priority of the planetary science community, these results have implications for the design of

315   landing and sampling systems for future landed missions to Enceladus and Europa. They also

316   highlight the importance of assessing and anticipating the surface properties via laboratory

317   studies and modeling to support the selection of candidate landing and sampling sites.

318

Acknowledgments

References

Anderson, J. D., Schubert, G., Jacobson, R. A., Lau, E. L., Moore, W. B., & Sjogren, W. L. (1998). Europa's Differentiated Internal Structure: Inferences from Four Galileo Encounters. *Science, 281*, 2019.

Arakawa, M., & Maeno, N. (1997). Mechanical strength of polycrystalline ice under uniaxial compression. *Cold regions science and technology, 26*(3), 215-229.

Berdis, J. R., Gudipati, M. S., Murphy, J. R., & Chanover, N. J. (2020). Europa's surface water ice crystallinity: Discrepancy between observations and thermophysical and particle flux modeling. *Icarus, 341*, 113660.

Bierhaus, E. B., Zahnle, K., Chapman, C. R., Pappalardo, R., McKinnon, W., & Khurana, K. (2009). Europa's crater distributions and surface ages. *Europa*, 161-180.

Blackford, J. R. (2007). TOPICAL REVIEW: Sintering and microstructure of ice: a review. *Journal of Physics D Applied Physics, 40*, R355.

Carey, E. M., Peters, G. H., Choukroun, M., Chu, L., Carpenter, E., Cohen, B., Panossian, L., Zhou, Y. M., Sarkissian, A., Moreland, S., Shiraishi, L. R., Backes, P., Zacny, K., Green, J. R., & Raymond, C. (2017). Development and characteristics of Mechanical Porous Ambient Comet Simulants as comet surface analogs. *Planetary and Space Science, 147*, 6-13.

Choukroun, M., Barmatz, M., & Castillo-Rogez, J. (2011). Understanding Evolution of Icy Satellites through Cryogenic Light Microscopy and Raman Studies. *Microscopy and Analysis-UK*(144), 5.

Filacchione, G., Capaccioni, F., Clark, R. N., Cuzzi, J. N., Cruikshank, D. P., Coradini, A., Cerroni, P., Nicholson, P. D., McCord, T. B., Brown, R. H., Buratti, B. J., Tosi, F., Nelson, R. M., Jaumann, R., & Stephan, K. (2010). Saturn's icy satellites investigated by Cassini-VIMS. II. Results at the end of nominal mission. *Icarus, 206*, 507.

Filacchione, G., Capaccioni, F., McCord, T. B., Coradini, A., Cerroni, P., Bellucci, G., Tosi, F., D'Aversa, E., Formisano, V., Brown, R. H., Baines, K. H., Bibring, J. P., Buratti, B. J., Clark, R. N., Combes, M., Cruikshank, D. P., Drossart, P., Jaumann, R., Langevin, Y., Matson, D. L., Mennella, V., Nelson, R. M., Nicholson, P. D., Sicardy, B., Sotin, C., Hansen, G., Hibbitts, K., Showalter, M., & Newman, S. (2007). Saturn's icy satellites investigated by Cassini-VIMS. I. Full-disk properties: 350 5100 nm reflectance spectra and phase curves. *Icarus, 186*, 259.

Glein, C. R., Baross, J. A., & Waite Jr, J. H. (2015). The pH of Enceladus' ocean. *Geochimica Et Cosmochimica Acta, 162*, 202-219.

Glein, C. R., Zolotov, M. Y., & Shock, E. L. (2008). The oxidation state of hydrothermal systems on early Enceladus. *Icarus, 197*(1), 157-163.

Hand, K. P. (2017). *Report of the Europa Lander science definition team*: National Aeronautics and Space Administration.

Hansen, G. B., & McCord, T. B. (2000). *Amorphous and Crystalline Ice on the Galilean Satellites: A Balance Between Thermal and Radiolytic Processes*. Paper presented at the Lunar and Planetary Science Conference. https://ui.adsabs.harvard.edu/abs/2000LPI....31.1630H

Howett, C., Spencer, J., Pearl, J., & Segura, M. (2010). Thermal inertia and bolometric Bond albedo values for Mimas, Enceladus, Tethys, Dione, Rhea and Iapetus as derived from Cassini/CIRS measurements. *Icarus, 206*(2), 573-593.

Iess, L., Stevenson, D., Parisi, M., Hemingway, D., Jacobson, R., Lunine, J., Nimmo, F., Armstrong, J., Asmar, S., & Ducci, M. (2014). The gravity field and interior structure of Enceladus. *Science, 344*(6179), 78-80.

Ingersoll, A. P., & Ewald, S. P. (2011). Total particulate mass in Enceladus plumes and mass of Saturn's E ring inferred from Cassini ISS images. *Icarus, 216*(2), 492-506.

Jia, X., Kivelson, M. G., Khurana, K. K., & Kurth, W. S. (2018). Evidence of a plume on Europa from Galileo magnetic and plasma wave signatures. *Nature astronomy, 2*, 459-464.

Kempf, S., Beckmann, U., & Schmidt, J. (2010). How the Enceladus dust plume feeds Saturn's E ring. *Icarus, 206*(2), 446-457.

McCallum, A. (2014). A brief introduction to cone penetration testing (CPT) in frozen geomaterials. *Annals of Glaciology, 55*(68), 7-14.

McCallum, A. B. (2012). *Cone penetration testing in polar snow*. University of Cambridge,

McKay, C., Davila, A., Glein, C., Hand, K., & Stockton, A. (2018). Enceladus astrobiology, habitability, and the origin of life. *Enceladus and the Icy Moons of Saturn; Schenk, PM, Clark, RN, Howett, CJA, Verbiscer, AJ, Waite, JH, Eds*, 437-452.

McKay, C. P., Anbar, A. D., Porco, C., & Tsou, P. (2014). Follow the plume: the habitability of Enceladus. *Astrobiology, 14*(4), 352-355.

McKay, C. P., Porco, C. C., Altheide, T., Davis, W. L., & Kral, T. A. (2008). The possible origin and persistence of life on Enceladus and detection of biomarkers in the plume. *Astrobiology, 8*(5), 909-919.

Molaro, J. L., Choukroun, M., Phillips, C. B., Phelps, E. S., Hodyss, R., Mitchell, K. L., Lora, J. M., & Meirion-Griffith, G. (2019). The Microstructural Evolution of Water Ice in the Solar System Through Sintering. *Journal of Geophysical Research (Planets), 124*, 243-277.

Nasello, O., de Juarez, S. N., & Di Prinzio, C. (2007). Measurement of self-diffusion on ice surface. *Scripta materialia, 56*(12), 1071-1073.

Paganini, L., Villanueva, G. L., Roth, L., Mandell, A., Hurford, T., Retherford, K. D., & Mumma, M. J. (2019). A measurement of water vapour amid a largely quiescent environment on Europa. *Nature astronomy*, 1-7.

Pappalardo, R. T., Senske, D. A., Prockter, L. M., Paczkowski, B., Vance, S., Goldstein, B., Magner, T., & Cooke, B. (2015). *Science and Reconnaissance from the Europa Clipper Mission Concept: Exploring Europa's Habitability*. Paper presented at the Lunar and Planetary Science Conference. https://ui.adsabs.harvard.edu/abs/2015LPI....46.2673P

Pappalardo, R. T., & Barr, A. C. (2004). The origin of domes on Europa: The role of thermally induced compositional diapirism. *Geophysical Research Letters, 31*(1).

Petrovic, J. J. (2003). Review Mechanical properties of ice and snow. *Journal of Materials Science, 38*(1), 1-6.

Porco, C. C., Dones, L., & Mitchell, C. (2017). Could it be snowing microbes on Enceladus? Assessing conditions in its plume and implications for future missions. *Astrobiology, 17*(9), 876-901.

Porco, C. C., Helfenstein, P., Thomas, P., Ingersoll, A., Wisdom, J., West, R., Neukum, G., Denk, T., Wagner, R., & Roatsch, T. (2006). Cassini observes the active south pole of Enceladus. *Science, 311*(5766), 1393-1401.

Postberg, F., Khawaja, N., Abel, B., Choblet, G., Glein, C. R., Gudipati, M. S., Henderson, B. L., Hsu, H.-W., Kempf, S., & Klenner, F. (2018). Macromolecular organic compounds from the depths of Enceladus. *Nature, 558*(7711), 564-568.

Postberg, F., Schmidt, J., Hillier, J., Kempf, S., & Srama, R. (2011). A salt-water reservoir as the source of a compositionally stratified plume on Enceladus. *Nature, 474*(7353), 620-622.

Postberg, F., Kempf, S., Schmidt, J., Brilliantov, N., Beinsen, A., Abel, B., Buck, U., & Srama, R. (2009). Sodium salts in E-ring ice grains from an ocean below the surface of Enceladus. *Nature, 459*(7250), 1098-1101.

Rogers, J. D. (2006). Subsurface exploration using the standard penetration test and the cone penetrometer test. *Environmental and Engineering Geoscience, 12*(2), 161-179.

Roth, L., Saur, J., Retherford, K. D., Strobel, D. F., Feldman, P. D., McGrath, M. A., & Nimmo, F. (2014). Transient Water Vapor at Europa's South Pole. *Science, 343*, 171-174.

Schmidt, J., Brilliantov, N., Spahn, F., & Kempf, S. (2008). Slow dust in Enceladus' plume from condensation and wall collisions in tiger stripe fractures. *Nature, 451*, 685.

Schubert, G., Anderson, J. D., Travis, B. J., & Palguta, J. (2007). Enceladus: Present internal structure and differentiation by early and long-term radiogenic heating. *Icarus, 188*(2), 345-355.

Schulson, E. M., & Duval, P. (2009). *Creep and fracture of ice*: Cambridge University Press.

Sekine, Y., Shibuya, T., Postberg, F., Hsu, H.-W., Suzuki, K., Masaki, Y., Kuwatani, T., Mori, M., Hong, P. K., & Yoshizaki, M. (2015). High-temperature water–rock interactions and hydrothermal environments in the chondrite-like core of Enceladus. *Nature Communications, 6*(1), 1-8.

Sohl, F., Choukroun, M., Kargel, J., Kimura, J., Pappalardo, R., Vance, S., & Zolotov, M. (2010). Subsurface Water Oceans on Icy Satellites: Chemical Composition and Exchange Processes. *Space Science Reviews, 153*(1-4), 485-510.

Sotin, C., & Tobie, G. (2004). Internal structure and dynamics of the large icy satellites. *Comptes Rendus Physique, 5*(7), 769-780.

Southworth, B. S., Kempf, S., & Spitale, J. (2019). Surface deposition of the Enceladus plume and the zenith angle of emissions. *Icarus, 319*, 33.

Sparks, W. B., Hand, K. P., McGrath, M. A., Bergeron, E., Cracraft, M., & Deustua, S. E. (2016). Probing for Evidence of Plumes on Europa with HST/STIS. *The Astrophysical Journal, 829*.

Spencer, J. R., & Nimmo, F. (2013). Enceladus: An active ice world in the Saturn system. *Annual Review of Earth and Planetary Sciences, 41*, 693-717.

Spencer, J. R., Tamppari, L. K., Martin, T. Z., & Travis, L. D. (1999). Temperatures on Europa from Galileo Photopolarimeter-Radiometer: Nighttime Thermal Anomalies. *Science, 284*, 1514.

Spitale, J. N., & Porco, C. C. (2007). Association of the jets of Enceladus with the warmest regions on its south-polar fractures. *Nature, 449*(7163), 695-697.

Suresh, S., & Naik, V. (2000). Hydrogen bond thermodynamic properties of water from dielectric constant data. *The Journal of Chemical Physics, 113*(21), 9727-9732.

441   van Herwijnen, A. (2013). Experimental analysis of snow micropenetrometer (SMP) cone penetration in
442   homogeneous snow layers. *Canadian geotechnical journal, 50*(10), 1044-1054.
443   Waite, J. H., Glein, C. R., Perryman, R. S., Teolis, B. D., Magee, B. A., Miller, G., Grimes, J., Perry, M. E., Miller,
444   K. E., & Bouquet, A. (2017). Cassini finds molecular hydrogen in the Enceladus plume: evidence for
445   hydrothermal processes. *Science, 356*(6334), 155-159.
446   Waite, J. H., Lewis, W., Magee, B., Lunine, J., McKinnon, W., Glein, C., Mousis, O., Young, D., Brockwell, T., &
447   Westlake, J. (2009). Liquid water on Enceladus from observations of ammonia and 40 Ar in the plume.
448   *Nature, 460*(7254), 487.
449   Zahnle, K., Alvarellos, J. L., Dobrovolskis, A., & Hamill, P. (2008). Secondary and sesquinary craters on Europa.
450   *Icarus, 194*, 660-674.
451   Zolotov, M. Y., & Kargel, J. S. (2009). On the Chemical Composition of Europa's Icy Shell, Ocean, and Underlying
452   Rocks. In *Europa* (pp. 431).
453   Zolotov, M. Y., & Shock, E. L. (2003). Energy for biologic sulfate reduction in a hydrothermally formed ocean on
454   Europa. *Journal of Geophysical Research (Planets), 108*.
455   Zolotov, M. Y., & Shock, E. L. (2001a). Composition and stability of salts on the surface of Europa and their
456   oceanic origin. *Journal of Geophysical Research, 106*, 32815-32828.
457   Zolotov, M. Y., & Shock, E. L. (2001b). *A hydrothermal origin for the sulfate-rich ocean of Europa.* Paper
458   presented at the Lunar and Planetary Science Conference.
459